



ELSEVIER

Contents lists available at [ScienceDirect](http://www.sciencedirect.com)

## Journal of Sound and Vibration

journal homepage: [www.elsevier.com/locate/jsv](http://www.elsevier.com/locate/jsv)

# Sound radiation by a moving line source above an impedance plane with frequency-dependent properties



D. Dragna\*, P. Blanc-Benon

Laboratoire de Mécanique des Fluides et d'Acoustique, UMR CNRS 5509, École Centrale de Lyon, Université de Lyon, 69134 Ecully Cedex, France

## ARTICLE INFO

## Article history:

Received 7 July 2014

Received in revised form

11 March 2015

Accepted 17 March 2015

Handling Editor: R.E. Musafir

Available online 7 April 2015

## ABSTRACT

An analytic solution for the problem of sound radiation by a harmonic line source moving at a uniform subsonic speed parallel to an impedance plane is proposed. The main originality of this work is that the variation of the impedance with the frequency is taken into account. Compared to the case of a constant impedance, the reflection coefficient and the location of its poles in the complex plane are modified. A uniform asymptotic expression is then developed for moderate Mach numbers and a closed-form expression, corresponding to a Weyl–Van der Pol formula, is proposed for a grazing incidence for hard grounds and for low Mach numbers. Unlike previous analytical solutions derived in the literature for a point-source, the impedance is evaluated at the Doppler frequency instead of at the source frequency. The analytical solution and asymptotic expressions are then compared satisfactorily to a numerical solution obtained from a time-domain solver of the linearized Euler equations. Finally, a parametric study is carried out showing that the assumption of a constant impedance is valid if the source Mach number remains small, typically less than 0.2, and if the source is not too close to the ground.

© 2015 Elsevier Ltd. All rights reserved.

## 1. Introduction

The rapid growth of computational power and recent developments in time-domain solvers offer new possibilities for investigating the acoustic radiation of moving sources outdoors. This is especially of interest in transportation noise studies. Indeed, time-domain solvers allow one to account for any trajectory or variation of the source speed during its motion. Recent studies [1,2] have demonstrated the feasibility of such simulations in complex environments. In addition, the outputs are time signals which can be used for auralization without additional post-processing. In order to validate the implementation of a moving source in these time-domain solvers, it is useful to have a benchmark. The analytical solutions proposed in the literature for the problem of sound radiation by moving sources above an impedance ground are however based on restrictive approximations.

Thus, for the most studied case which is the radiation of a harmonic source moving at a constant speed and at a constant height above a flat ground, two assumptions are widely employed. The first one consists in neglecting the singularities of the reflection coefficient [3,4]. Therefore, the asymptotic solutions proposed at a long range at the first-order in [3,4] neglect the so-called ground wave. However, for a non-moving source, the ground wave is an important contribution at low frequencies

\* Corresponding author.

E-mail addresses: [didier.dragna@ec-lyon.fr](mailto:didier.dragna@ec-lyon.fr) (D. Dragna), [philippe.blanc-benon@ec-lyon.fr](mailto:philippe.blanc-benon@ec-lyon.fr) (P. Blanc-Benon).

<b>Nomenclature</b>		$\delta$	Dirac delta function
<i>Latin characters</i>		$\gamma$	$(1 - M^2)^{-1/2}$
$b$	impulse response of the admittance $\beta$	$\theta$	polar angle centered at the image source
$B$	boundary loss factor function	$\rho_0$	air density
$c_0$	sound speed	$\sigma_0$	air flow resistivity
$d$	distance between the source and the receiver	$\varphi$	acoustic potential
$f_0$	emitting frequency	$\psi$	polar angle centered at the source
$k_0 = \omega_0/c_0$	wavenumber	$\omega$	angular frequency
$k_p$	pole of the reflection coefficient	$\omega_0$	$2\pi f_0$
$k$	Fourier variable	<i>Subscripts</i>	
$k_s$	saddle point	$D$	refers to the direct wave
$l$	thickness in the surface admittance model	$e$	quantity evaluated at the emission time
$p$	acoustic pressure	$L$	quantity in the Lorentz space
$M = V_s/c_0$	Mach number	$p$	refers to the poles of the reflection coefficient
$n$	numerical distance	$R$	refers to the reflected wave
$r$	distance between the image source and the receiver	$sd$	quantity evaluated along the steepest descent path
$R$	reflection coefficient	$S$	refers to surface waves
$R_s$	reflection coefficient evaluated at the saddle point	<i>Superscripts</i>	
$t$	time	$\pm$	refers to the two poles originating from the poles of the reflection coefficient for $M=0$
$\mathbf{v} = (v_x, v_z)$	acoustic velocity	<i>Special functions</i>	
$V_s$	source speed	erfc	complementary error function
$(x, z)$	spatial coordinates	$H$	Heaviside function
$(x_s, z_s)$	spatial coordinates of the source	$H_\nu^{(1)}$	Hankel function of the first kind of order $\nu$
<i>Greek characters</i>			
$\alpha$	$\sqrt{k_0^2 - k^2}$		
$\beta$	normalized surface admittance		

when the source and the receivers are close to the ground (see, e.g. [5]). The second assumption is that the ground properties are equal to those at the source frequency and, therefore, do not depend on the frequency for a harmonic source [3,6], as noticed by Ochmann [7]. However, while the emitting frequency for a harmonic source is constant, the frequency of the acoustic waves impacting the ground is modified due to the well-known Doppler effect. Therefore, a significant error can be expected as most natural grounds have frequency-dependent properties. Recently, analytical solutions have been proposed without these two assumptions [7] but only for simple impedance models.

The present paper is concerned with the acoustic radiation of a harmonic line source moving at a constant subsonic speed and at a constant height above an impedance plane, with a frequency-dependent impedance. The main objectives are to determine the analytical solution and to propose a uniform asymptotic expression in the acoustic far field. The combined effects of the source motion and of a frequency-dependent impedance on the reflection coefficient and on its poles are discussed. The proposed solution could be used as a benchmark for time-domain solvers.

The paper is organized as follows. In Section 2, the problem is described and an analytical solution is expressed in an integral form. In Section 3, an asymptotic analysis is conducted, and, for a grazing incidence, a closed-form expression is derived for low Mach numbers and for hard grounds. These various analytical solutions are compared in Section 4 to a numerical solution obtained from a time-domain solver of the linearized Euler equations. Finally, in Section 5, the importance of accounting for the frequency variation of the ground properties is emphasized.

## 2. Analytical solution

In the physical coordinate system  $(x, z, t)$ , the line source is moving at a constant height  $z_s$  and at a constant subsonic speed  $V_s = Mc_0$ , where  $M$  is the Mach number with  $M < 1$  and  $c_0$  is the sound speed in the air. The schematic of the problem is depicted in Fig. 1. The acoustic equations are given by

$$\frac{\partial p}{\partial t} + \rho_0 c_0^2 \nabla \cdot \mathbf{v} = \rho_0 c_0^2 \delta(x - Mc_0 t) \delta(z - z_s) e^{-i\omega_0 t}, \quad (1)$$

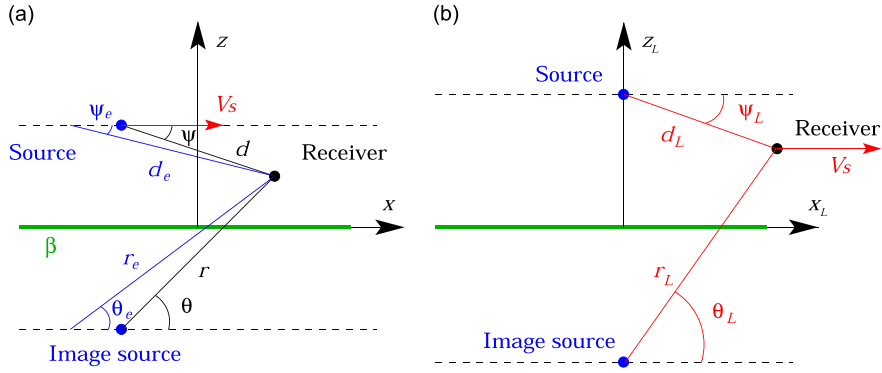


Fig. 1. Moving line-source above an impedance plane (a) in the physical space and (b) in the Lorentz space.

$$\rho_0 \frac{\partial \mathbf{v}}{\partial t} + \nabla p = 0, \tag{2}$$

with  $p$  and  $\mathbf{v} = (v_x, v_z)$  being the acoustic pressure and velocity and with  $\omega_0 = 2\pi f_0$  where  $f_0$  is the emitting frequency. The air density  $\rho_0$  and the sound speed in the air are constant and their values are  $\rho_0 = 1.2 \text{ kg m}^{-3}$  and  $c_0 = 340 \text{ m s}^{-1}$ . Introducing the acoustic potential  $\varphi$  such as  $p = -\rho_0 \partial\varphi/\partial t$  and  $\mathbf{v} = \nabla\varphi$ , Eq. (1) becomes

$$\Delta\varphi - \frac{1}{c_0^2} \frac{\partial^2 \varphi}{\partial t^2} = \delta(x - Mc_0t)\delta(z - z_s)e^{-i\omega_0t}. \tag{3}$$

At the ground, the impedance or the admittance boundary condition is satisfied, leading to

$$\rho_0 c_0 v_z(x, z = 0, t) + \int_{-\infty}^{+\infty} b(u)p(x, z = 0, t - u) du = 0, \tag{4}$$

where the impulse response  $b(t)$  is related to the surface admittance  $\beta(\omega)$  by the Fourier transform:

$$\beta(\omega) = \int_{-\infty}^{+\infty} b(t)e^{i\omega t} dt. \tag{5}$$

The admittance boundary condition for the acoustic potential is then

$$c_0 \frac{\partial \varphi}{\partial z}(x, z = 0, t) - \int_{-\infty}^{+\infty} b(u) \frac{\partial \varphi}{\partial t}(x, z = 0, t - u) du = 0. \tag{6}$$

As an admittance boundary condition is considered, this study is restricted to locally reacting grounds.

### 2.1. Modified Lorentz transform

To reduce the problem to the case of a non-moving source, we introduce the modified Lorentz transform [8,3,6,7]

$$x_L = \gamma^2(x - Mc_0t), \tag{7}$$

$$z_L = \gamma z, \tag{8}$$

$$t_L = \gamma^2 \left( t - M \frac{x}{c_0} \right), \tag{9}$$

with  $\gamma = 1/\sqrt{1 - M^2}$ . Using a chain rule expansion for the calculation of the derivatives:

$$\frac{\partial}{\partial t} = \gamma^2 \frac{\partial}{\partial t_L} - \gamma^2 M c_0 \frac{\partial}{\partial x_L}, \tag{10}$$

$$\frac{\partial}{\partial x} = -\frac{\gamma^2 M}{c_0} \frac{\partial}{\partial t_L} + \gamma^2 \frac{\partial}{\partial x_L}, \tag{11}$$

$$\frac{\partial}{\partial z} = \gamma \frac{\partial}{\partial z_L}, \tag{12}$$

the wave equation in Eq. (3) is written in the Lorentz space as

$$\left[ \frac{\partial^2}{\partial x_L^2} + \frac{\partial^2}{\partial z_L^2} - \frac{1}{c_0^2} \frac{\partial^2}{\partial t_L^2} \right] \varphi = \gamma \delta(x_L) \delta(z_L - z_{L,S}) e^{-i\omega_0 t_L}, \tag{13}$$

with  $z_{L,S} = \gamma z_S$ . The solution can then be sought as a time-harmonic solution  $\varphi(x_L, z_L, t_L) = \tilde{\varphi}(x_L, z_L)e^{-i\omega_0 t_L}$ , whose amplitude  $\tilde{\varphi}$  satisfies the equation:

$$\left[ \frac{\partial^2}{\partial x_L^2} + \frac{\partial^2}{\partial z_L^2} + k_0^2 \right] \tilde{\varphi} = \gamma \delta(x_L) \delta(z_L - z_{L,S}), \tag{14}$$

with the wavenumber  $k_0 = \omega_0/c_0$ . Introducing a Fourier transform along the  $x_L$ -direction:

$$\hat{\varphi}(k, z_L) = \int_{-\infty}^{+\infty} \tilde{\varphi}(x_L, z_L) e^{-ikx_L} dx_L, \tag{15}$$

Eq. (14) becomes

$$\left[ \frac{d^2}{dz_L^2} + (k_0^2 - k^2) \right] \hat{\varphi} = \gamma \delta(z_L - z_{L,S}). \tag{16}$$

Concerning the admittance boundary condition, it is first written in the Lorentz space from Eq. (6) as

$$c_0 \gamma \frac{\partial \varphi}{\partial z_L}(x_L, z_L = 0, t_L) - \int_{-\infty}^{+\infty} b(u) \gamma^2 \left[ \frac{\partial}{\partial t_L} - M c_0 \frac{\partial}{\partial x_L} \right] \varphi(x_L + M c_0 \gamma^2 u, z_L = 0, t_L - \gamma^2 u) du = 0. \tag{17}$$

This becomes for the amplitude  $\tilde{\varphi}$  of the acoustic potential  $\varphi$ :

$$c_0 \frac{\partial \tilde{\varphi}}{\partial z_L}(x_L, z_L = 0) + \int_{-\infty}^{+\infty} b(u) \gamma \left[ i\omega_0 + M c_0 \frac{\partial}{\partial x_L} \right] \tilde{\varphi}(x_L + M c_0 \gamma^2 u, z_L = 0) e^{i\omega_0 \gamma^2 u} du = 0. \tag{18}$$

Introducing the Fourier transform along the  $x_L$ -direction, one obtains

$$\frac{d\hat{\varphi}}{dz_L}(k, z_L = 0) + (ik_0 + ikM) \gamma \hat{\varphi}(k, z_L = 0) \int_{-\infty}^{+\infty} b(u) e^{i(\omega_0 + kc_0 M) \gamma^2 u} du = 0, \tag{19}$$

which finally leads to the boundary condition

$$\frac{d\hat{\varphi}}{dz_L}(k, z_L = 0) + i(k_0 + kM) \gamma \beta [(\omega_0 + kc_0 M) \gamma^2] \hat{\varphi}(k, z_L = 0) = 0. \tag{20}$$

### 2.2. Solution

As the study is restricted to subsonic sources, only progressives waves are considered [8]. The solution is then sought in the form

$$\hat{\varphi}_1 = A e^{i\alpha z_L} + B e^{-i\alpha z_L} \quad \text{for } 0 \leq z_L \leq z_{L,S}, \tag{21}$$

$$\hat{\varphi}_2 = C e^{i\alpha z_L} \quad \text{for } z_{L,S} \leq z_L, \tag{22}$$

with  $\alpha = \sqrt{k_0^2 - k^2}$ . The constants  $A$ ,  $B$  and  $C$  are determined by the conditions:

$$\hat{\varphi}_1(k, z_{L,S}) = \hat{\varphi}_2(k, z_{L,S}), \tag{23}$$

$$\frac{d\hat{\varphi}_2}{dz_L}(k, z_{L,S}) - \frac{d\hat{\varphi}_1}{dz_L}(k, z_{L,S}) = \gamma, \tag{24}$$

$$\frac{d\hat{\varphi}_1}{dz_L}(k, z_L = 0) + i(k_0 + kM) \gamma \beta [(\omega_0 + kc_0 M) \gamma^2] \hat{\varphi}_1(k, z_L = 0) = 0. \tag{25}$$

The first condition expresses the continuity of  $\hat{\varphi}$  at the source height. The second condition is related to the discontinuity of the derivative of  $\hat{\varphi}$  at the source height and is obtained by integrating Eq. (16) over a small interval  $z_L$  around  $z_{L,S}$ . Finally, the third condition is the admittance boundary condition given in Eq. (20).

Eqs. (23)–(25) lead to the solution:

$$\hat{\varphi} = \frac{\gamma}{2i\alpha} \left[ e^{i\alpha|z_L - z_{L,S}|} + R(k) e^{i\alpha(z_L + z_{L,S})} \right], \tag{26}$$

with the reflection coefficient:

$$R(k) = \frac{\alpha - (k_0 + kM) \gamma \beta [(\omega_0 + kc_0 M) \gamma^2]}{\alpha + (k_0 + kM) \gamma \beta [(\omega_0 + kc_0 M) \gamma^2]}. \tag{27}$$

This reflection coefficient is similar to that obtained in previous studies for a point source moving above an admittance plane whose admittance is constant with the frequency [3,6], except that the admittance is now a function of  $k$  and  $M$ . The acoustic potential in the Lorentz space is then written as

$$\varphi(x_L, z_L) = \frac{1}{2\pi} \int_{-\infty}^{+\infty} \hat{\varphi}(k, z_L) e^{ikx_L} dk e^{-i\omega_0 t_L}, \tag{28}$$

which can be split into  $\varphi = \varphi_D + \varphi_R$ :

$$\varphi_D(x_L, z_L) = \frac{1}{2\pi} \int_{-\infty}^{+\infty} \frac{\gamma}{2i\alpha} e^{ikx_L + i\alpha|z_L - z_{L,S}|} dk e^{-i\omega_0 t_L} = -\frac{i}{4} \gamma H_0^{(1)}(k_0 d_L) e^{-i\omega_0 t_L}, \tag{29}$$

$$\varphi_R(x_L, z_L) = \frac{1}{2\pi} \int_{-\infty}^{+\infty} \frac{\gamma}{2i\alpha} R(k) e^{ikx_L + i\alpha h_L} dk e^{-i\omega_0 t_L}. \tag{30}$$

In the preceding equations, the notations  $d_L = \sqrt{x_L^2 + (z_L - z_{L,S})^2}$  and  $h_L = (z_L + z_{L,S})$  have been introduced.

The acoustic pressure is then obtained from the relation  $p = -\rho_0 \partial\varphi/\partial t$ , which leads to, using Eq. (10):

$$p = -\rho_0 \gamma^2 \frac{\partial\varphi}{\partial t_L} + \rho_0 \gamma^2 M c_0 \frac{\partial\varphi}{\partial x_L}. \tag{31}$$

The acoustic pressure can also be split into  $p = p_D + p_R$ , where  $p_D$  is the direct wave:

$$p_D(x_L, z_L) = \rho_0 c_0 \frac{k_0 \gamma^3}{4} e^{-i\omega_0 t_L} \left( H_0^{(1)}(k_0 d_L) + iM \cos\psi_L H_1^{(1)}(k_0 d_L) \right), \tag{32}$$

with  $\cos\psi_L = x_L/d_L$ , and  $p_R$  is the reflected wave:

$$p_R(x_L, z_L) = \rho_0 c_0 \frac{\gamma^3}{2\pi} \int_{-\infty}^{+\infty} \frac{(k_0 + kM)}{2\alpha} R(k) e^{ikx_L + i\alpha h_L} dk e^{-i\omega_0 t_L}. \tag{33}$$

The numerical evaluation of the reflected wave  $p_R$  is complicated by the oscillatory behavior of the integrand. To have a reasonable computational time, an asymptotic solution in the acoustic far field is developed in the next section.

### 3. Asymptotic expression in the acoustic far field

Before turning to the asymptotic evaluation of the reflected wave, an asymptotic formula is proposed for the direct wave  $p_D$ . It is obtained straightforwardly from the asymptotic expressions of the Hankel functions [9] under the restriction  $z \gg 1$ :

$$H_\nu^{(1)}(z) = \sqrt{\frac{2}{\pi z}} e^{iz - i\nu\pi/2 - i\pi/4}. \tag{34}$$

This leads to, for  $k_0 d_L \gg 1$ :

$$p_D(x_L, z_L) = \rho_0 c_0 \frac{k_0 \gamma^3}{4} \frac{e^{-i\omega_0 t_L + ik_0 d_L}}{\sqrt{ik_0 d_L}} \sqrt{\frac{2}{\pi}} (1 + M \cos\psi_L). \tag{35}$$

#### 3.1. Steepest descent path

A standard method for the asymptotic evaluation of  $p_R$  is the steepest descent method. It has been used extensively in the literature, especially for the problem of radiation of acoustic waves above an impedance plane (see, e.g., [10–18]). Details on the method can be found in [19–21]. Firstly, the saddle points of the phase function in the integrand of Eq. (33)  $Q(k) = ikx_L + i\alpha h_L$  are determined by requiring that  $dQ/dk = 0$ . In this case, there is only one saddle point, as the equality  $dQ/dk = 0$  is satisfied only for  $k_s = k_0 x_L/r_L$ , with  $r_L = \sqrt{x_L^2 + h_L^2}$ . Corresponding values of  $\alpha$  and  $Q(k)$  are  $\alpha(k_s) = k_0 h_L/r_L$  and  $Q(k_s) = ik_0 r_L$ . The steepest descent path is then obtained from the relation

$$Q(k_{sd}(q)) = Q(k_s) - k_0 r_L q^2, \tag{36}$$

with  $q$  being real. To get the value of  $k$  along the steepest descent path, denoted by  $k_{sd}(q)$ , the preceding relation must be inverted. For that, Eq. (36) is rewritten as

$$\alpha(k_{sd}(q))h_L = -k_{sd}(q)x_L + k_0 r_L (1 + iq^2). \tag{37}$$

By taking the square of the preceding equation, one obtains a quadratic equation which gives the steepest descent path:

$$k_{sd}(q) = k_0 \cos\theta_L (1 + iq^2) - iqk_0 \sin\theta_L \sqrt{2i - q^2}, \tag{38}$$

$$\alpha_{sd}(q) = k_0 \sin\theta_L (1 + iq^2) + iqk_0 \cos\theta_L \sqrt{2i - q^2}, \tag{39}$$

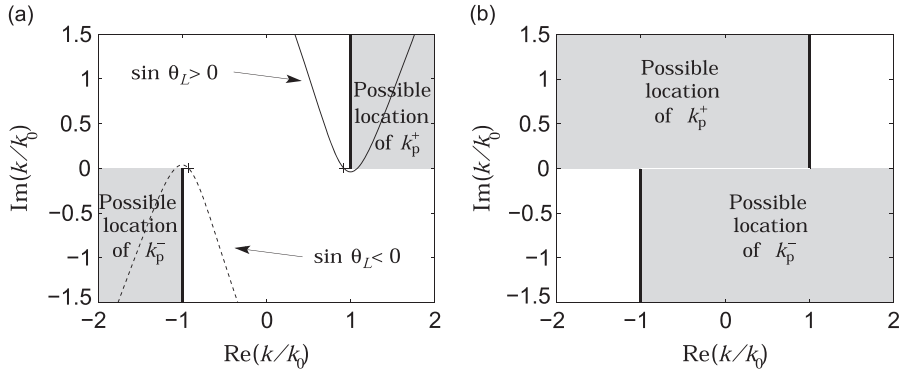


**Fig. 2.** Branch cuts of the function  $\alpha(k) = \sqrt{k_0^2 - k^2}$  in the first (a) and second sheet (b) of the  $k$ -plane (thick solid lines). The steepest descent path obtained for  $\theta_L = \pi/8$  (solid line) and  $\theta_L = 7\pi/8$  (dashed line) and the corresponding saddle points (crosses) are also represented in the first sheet. The gray regions correspond to the possible location of the poles in the two sheets.

with  $\cos\theta_L = x_L/r_L$  and  $\sin\theta_L = h_L/r_L$ . The branch cut of the square-root function is chosen as the real negative axis so that the contour is traversed in the correct direction [18]. Examples of steepest descent paths obtained for  $\sin(\theta_L) > 0$  and  $\sin(\theta_L) < 0$  have been represented in the  $k$ -plane in Fig. 2. It has a parabola shape and is located in the upper half-plane if  $\sin(\theta_L) > 0$  and in the lower half-plane if  $\sin(\theta_L) < 0$ .

The initial integration path can then be deformed into the steepest descent path. The branch cuts of the function  $\alpha$  are chosen as depicted in Fig. 2(a) so that they are not crossed during the deformation of the integration contour [18]. This defines two sheets of the  $k$ -plane forming a Riemann surface. On the first sheet, which is the physical sheet, the function  $\alpha$  is positive for  $-k_0 < k < k_0$ , while on the second sheet, it is negative. Note that the integration is performed in the first sheet of the  $k$ -plane.

### 3.2. Discussion on the poles of the reflection coefficient

During the deformation of the integration path, singularities of the reflection coefficient, which are poles or branch points, can be crossed. They will add contributions to the reflected wave. The location of the poles in the  $k$ -plane is obtained from the zeros of the denominator of the reflection coefficient:

$$D(\omega_0, k, M) = \alpha + (k_0 + kM)\gamma\beta[(\omega_0 + kc_0M)\gamma^2] = 0. \tag{40}$$

The solution of the preceding equation is known for two values of  $M$ . For  $M=0$ , corresponding to the well-established case of a non-moving line source, there are two poles located at  $(k_p^- = -k_0\sqrt{1-\beta^2}, \alpha_p^- = -k_0\beta)$  and  $(k_p^+ = k_0\sqrt{1-\beta^2}, \alpha_p^+ = -k_0\beta)$ . The poles are located in the first sheet of the function  $\alpha$  if  $\text{Im}[\beta] < 0$  and  $|\text{Re}[\sqrt{1-\beta^2}]| > 1$  and in the second sheet if  $\text{Im}[\beta] > 0$  or if  $\text{Im}[\beta] < 0$  and  $|\text{Re}[\sqrt{1-\beta^2}]| < 1$ . Note that in this last case, the poles are never crossed for any value of  $\theta_L$ . For  $M=1$ , there is only one possible solution for Eq. (40) which is  $k_p = -k_0$  and  $\alpha_p = 0$ .

If the admittance does not depend on the frequency, there are still only two poles. Indeed, the solutions of  $D(\omega_0, k, M) = 0$  can be obtained explicitly in this case. For that, Eq. (40) is rewritten as the quadratic equation  $k_0^2 - k^2 - (k_0 + kM)^2\gamma^2\beta^2 = 0$ , whose solutions are

$$k_p^\pm = \pm k_0 \frac{\sqrt{1-\beta^2} \mp M}{1 \mp M\sqrt{1-\beta^2}}, \tag{41}$$

$$\alpha_p^\pm = -k_0 \frac{\beta}{\gamma(1 \mp M\sqrt{1-\beta^2})}. \tag{42}$$

For  $M=0$ , the wavenumbers of the surface waves in the horizontal and vertical directions are retrieved. For  $M=1$ , the two poles coalesce into  $k_p = -k_0$  and  $\alpha_p = 0$ . The trajectory of the poles  $k_p^\pm$  in the complex plane is a circle whose radius  $R$  and center  $C^\pm$  are given by, for hard grounds  $|\beta|^2 \ll 1$ :

$$R = \frac{k_0}{2} \left( \frac{|\text{Re}[\beta]|}{|\text{Im}[\beta]|} + \frac{|\text{Im}[\beta]|}{|\text{Re}[\beta]|} \right), \tag{43}$$

$$C^\pm = \pm \frac{ik_0}{2} \left( \frac{\text{Re}[\beta]}{|\text{Im}[\beta]|} - \frac{\text{Im}[\beta]}{|\text{Re}[\beta]|} \right), \tag{44}$$

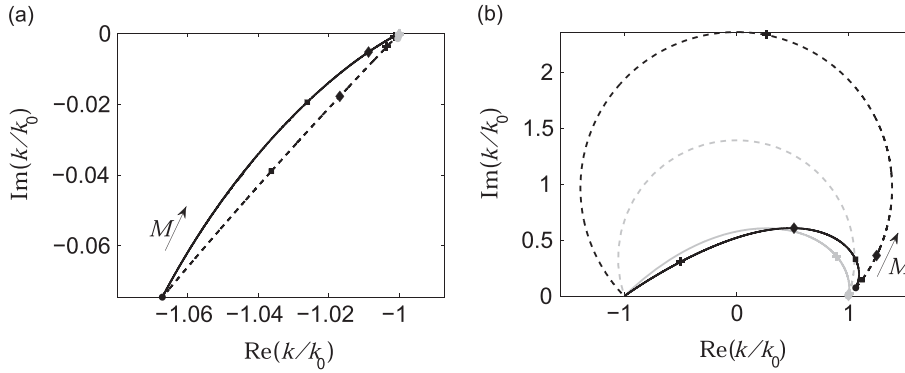


**Fig. 3.** Trajectory of the poles (a)  $k_p^-$  and (b)  $k_p^+$  in the  $k$ -plane for Mach numbers between 0 and 1 obtained (solid line) assuming a frequency-varying admittance and (dashed line) a constant admittance. The admittance model is in black lines the Miki model of a rigidly backed layer with  $\sigma_0 = 10 \text{ kPa s m}^{-2}$  and  $l=0.1 \text{ m}$  and in gray lines the Miki model of a semi-infinite ground layer with  $\sigma_0 = 500 \text{ kPa s m}^{-2}$ . The emitting frequency is  $f_0 = 200 \text{ Hz}$ . The symbols  $\bullet$ ,  $\blacksquare$ ,  $\blacklozenge$  and  $+$  correspond to the values obtained for  $M=0, 0.3, 0.6$  and  $0.9$ .

where  $\text{Re}(z)$  and  $\text{Im}(z)$  denote the real and imaginary parts of a complex number  $z$ . Examples in this paper are shown using the modified Miki model of a rigidly backed layer of thickness  $l$  and of air flow resistivity  $\sigma_0$  [22,23]:

$$\beta(\omega) = \beta_\infty \tanh(-ik_c l), \tag{45}$$

with

$$\beta_\infty(\omega) = 1 / \left[ 1 + 0.459 \left( \frac{\sigma_0}{-i\rho_0\omega} \right)^{0.632} \right], \tag{46}$$

$$k_c(\omega) = k_0 \left[ 1 + 0.643 \left( \frac{\sigma_0}{-i\rho_0\omega} \right)^{0.632} \right]. \tag{47}$$

The Miki model and other related one-parameter impedance models have limited applications for outdoor grounds. As shown in Attenborough et al. [24], they provide less accurate comparisons with experimental data than more complex impedance models such as the relaxation model [25] or the slit-pore model [24]. However, one-parameter impedance models are widespread for surface transportation noise studies, as they are used for instance in the Harmonoise model for predicting road traffic noise and railway noise [26]. Moreover, they capture the essential of the physics. Therefore, a one-parameter impedance model, i.e. the Miki model, is used in the study. The poles trajectory is depicted in Fig. 3 for two admittance models. In the first model, represented in a dashed black line, a rigidly backed layer with  $\sigma_0 = 10 \text{ kPa s m}^{-2}$  and  $l=0.1 \text{ m}$  is considered. In the second one, represented in a gray dashed line, a semi-infinite ground with  $\sigma_0 = 500 \text{ kPa s m}^{-2}$  is considered. In both cases, the emitted frequency is  $f_0 = 200 \text{ Hz}$ . Under the assumption of a constant admittance, it is seen that the trajectory of the poles  $k_p^\pm$  is a circle connecting the points  $\pm k_0 \sqrt{1 - \beta^2}$  obtained for  $M=0$  and  $-k_0$  obtained for  $M=1$ . Note also that  $k_p^-$  and  $k_p^+$  are located in the lower and upper half-plane, respectively. In addition, the location of the pole  $k_p^-$  for the second admittance model does not vary too much from its value at  $M=0$  as the Mach number increases. Indeed, the value of  $k_p^-$  at  $M=0$  is close to that at  $M=1$ , which is  $-k_0$ .

For a frequency-varying admittance, it is not possible to give an analytical expression of the poles in the general case. An approximate formula for low Mach numbers is proposed later in Section 3.5.2. It is assumed thereafter that for  $M > 0$ , there are also two poles or that contributions of the other poles are negligible. As most admittance models for outdoor ground surfaces have a negative imaginary part (see, e.g., [5,24]), the study is thereafter restricted to  $\text{Im}[\beta(\omega)] < 0$  for  $\omega > 0$  for simplification purposes. Note also that for  $k$  real and  $M \neq 1$ , a solution of Eq. (40) is possible only if  $\beta$  is an imaginary number or a real number, as  $\alpha$  is real or imaginary for  $k$  real. As usually  $\text{Re}[\beta(\omega)] > 0$  and as it is assumed that  $\text{Im}[\beta(\omega)] < 0$  for  $\omega > 0$ , the poles cannot cross the real axis of the  $k$ -plane in both sheets. Therefore, for  $M < 1$ , the poles  $k_p^-$  and  $k_p^+$  are confined in the gray regions of the  $k$ -plane represented in Fig. 2.

As  $\text{Im}[q] = 0$ , with  $q$  defined by Eq. (36), on the steepest descent path,  $\text{Im}[q]$  appears as a suitable parameter to determine whether the poles are crossed. As a function of  $\alpha$ , the function  $q$  is defined on a four-sheeted  $k$ -plane. The position of the poles in the  $q$ -plane is denoted by  $q_p$ . As discussed in [21], the function  $q$  must be determined so that the position of the saddle point is similar in the  $k$ -plane and in the  $q$ -plane. Denoting by  $Q'$  the second derivative of  $Q$  with respect to  $k$ , this is mathematically written as  $(k_p - k_s)/q_p \rightarrow \sqrt{-2/Q''(k_s)}$  as  $k_p \rightarrow k_s$ , where  $\arg \sqrt{-2/Q''(k_s)} = -\pi/4$  in this case [20]. By checking carefully this condition in the various regions of the physical sheet in the  $k$ -plane, the values of  $q$  at the poles are thus

defined by

$$q_p^- = -\sqrt{i - ik_p^-/k_0 \cos \theta_L - i\alpha_p^-/k_0 \sin \theta_L}, \tag{48}$$

$$q_p^+ = \sqrt{i - ik_p^+/k_0 \cos \theta_L - i\alpha_p^+/k_0 \sin \theta_L}. \tag{49}$$

In that case, in the physical sheet of the  $k$ -plane,  $\text{Im}[q_p]$  is positive if it is located above the steepest descent path and negative if it is located below. If the poles  $k_p^-$  and  $k_p^+$  are not in the physical sheet, they are however located on sheets where  $\text{Im}[q_p^-] < 0$  and  $\text{Im}[q_p^+] > 0$ , respectively. Therefore, the condition for the poles  $k_p^-$  and  $k_p^+$  to be crossed is simply that  $\text{Im}[q_p^-] > 0$  and  $\text{Im}[q_p^+] < 0$ .

Note also that the function  $\beta(\omega)$  can have some singularities. For causality reasons,  $\beta(\omega)$  is analytic in the upper half  $\omega$ -plane [27] and the singularities can only be located in the lower half  $\omega$ -plane. It is also assumed that the contributions due to these singularities can be neglected. For instance, the half-line of imaginary numbers with a negative imaginary part is a branch cut in the  $\omega$ -plane for the Miki model extended to the complex plane [22,23]. In the  $k$ -plane, this branch cut is located at  $\text{Re}[k] = -k_0/M$  and  $\text{Im}[k] \leq 0$ . Therefore, it is assumed that  $M$  is not too large so that the contributions of these singularities are far from the saddle point and can be omitted.

A numerical method based on the Newton–Raphson algorithm [28] is employed to determine the location of the poles  $k_p^-$  and  $k_p^+$  in the complex  $k$ -plane. It is obtained iteratively by starting from the known solutions for  $M=0$  and by incrementing  $M$  by small steps using the previous solution as the trial solution of the relation  $D(\omega_0, k, M) = 0$  to the desired value of the Mach number. For the same configurations that discussed above, the poles trajectory obtained by accounting for the frequency variation of the admittance is represented in Fig. 3. In that case, the trajectory is not a circle. The positions of the poles in the complex plane can then be dramatically modified. For instance, for the Miki model of a rigidly backed layer with  $\sigma_0 = 10 \text{ kPa s m}^{-2}$  and  $l=0.1 \text{ m}$  and for an emitting frequency  $f_0 = 200 \text{ Hz}$ , the pole  $k_p^+$  for  $M=0.3$  is located at  $k_p^+/k_0 = 1.12 + 0.15i$  if the admittance is supposed to be a constant and at  $k_p^+/k_0 = 1.07 + 0.33i$  if the frequency variation is accounted for.

Note that the method provides only the location of the two poles originating from the poles of the reflection coefficient for  $M=0$ . To account for all the poles, one possible method is to approximate the admittance by a rational function (see, e.g., [29,30]) and to rewrite the relation  $D(\omega_0, k, M) = 0$  as a polynomial equation. The poles can then be deduced from the zeros of this polynomial equation. As an example, the trajectory of the poles are represented in Fig. 4 in the  $k$ -plane as  $M$  increases for three Mach numbers. The corresponding values of the poles  $k_p^\pm$  are given in Table 1. The admittance model is the Miki model with parameters  $\sigma_0 = 100 \text{ kPa s m}^{-2}$  and  $l = \infty$ , and the emitting frequency is  $f_0 = 200 \text{ Hz}$ . A fourth degree rational function, whose coefficients can be found in Cotté et al. [31], is used to approximate the admittance.

Therefore, there are in this case ten poles. For  $M=0.3$ , there are only two poles located close to the real axis, corresponding to  $k_p^-$  and  $k_p^+$ . As indicated in Table 1, the location of the poles is only slightly changed for this Mach number.

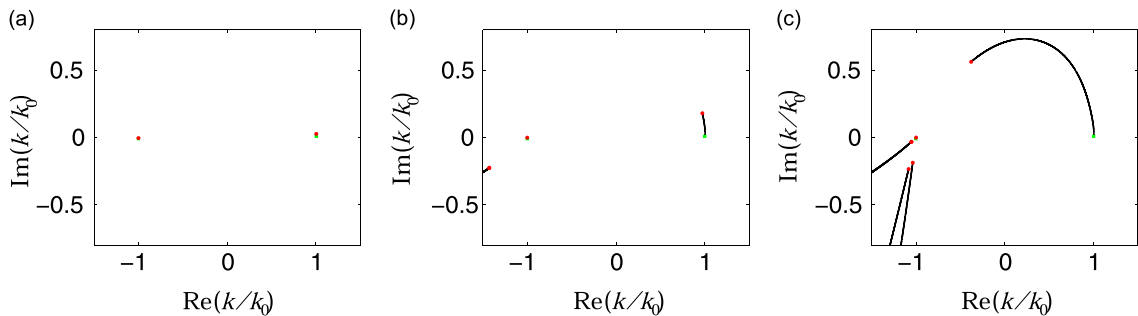


**Fig. 4.** Trajectories of the poles in the  $k$ -plane for the Miki admittance model of a semi-infinite ground of air flow resistivity  $\sigma_0 = 100 \text{ kPa s m}^{-2}$  as the Mach number increases from the initial value at  $M=0$  represented by a green square to the final value at (a)  $M=0.3$ , (b)  $0.7$  and (c)  $0.95$  represented by a red dot. The emitting frequency is set to  $f_0 = 200 \text{ Hz}$ . (For interpretation of the references to color in this figure caption, the reader is referred to the web version of this paper.)

**Table 1**

Values of the poles of the reflection coefficient  $k_p^\pm$  for four Mach numbers obtained using the Miki admittance model of a semi-infinite ground of air flow resistivity  $\sigma_0 = 100 \text{ kPa s m}^{-2}$  and a source frequency  $f_0 = 200 \text{ Hz}$ .

	$M=0$	$M=0.3$	$M=0.7$	$M=0.95$
$k_p^+/k_0$	$1.002 + 0.010i$	$1.003 + 0.028i$	$0.973 + 0.181i$	$-0.379 + 0.563i$
$k_p^-/k_0$	$-1.002 - 0.010i$	$-1.001 - 0.004i$	$-1.000 - 0.001i$	$-1.000 - 0.000i$

Therefore, the poles obtained for  $M=0.3$  are very close to those obtained for  $M=0$ , as seen in Fig. 4(a). The other eight poles have a large imaginary part and the contributions of the related surface waves to the reflected wave are negligible. For  $M=0.7$ , the pole  $k_p^-$  is located closer to the real axis, while  $k_p^+$  moves away from it. In addition, two other poles can be observed around  $k/k_0 = -1.3 - 0.2i$  in Fig. 4(b). As  $M$  tends to one, all the poles go close to  $k = -k_0$ . Therefore, for  $M=0.95$ , six of the ten poles can be distinguished in Fig. 4(c). In particular, the two additional poles observed for  $M=0.7$  come closer to the real axis. In that case, contributions from the poles other than  $k_p^-$  and  $k_p^+$  cannot be neglected.

### 3.3. Deformation of the contour

Under the assumptions presented previously, the reflected wave is written from Eq. (33) as

$$p_R(x_L, z_L) = p_{R,sd}(x_L, z_L) + H[\text{Im}(q_p^-)]p_S^-(x_L, z_L) + H[-\text{Im}(q_p^+)]p_S^+(x_L, z_L), \tag{50}$$

where  $p_{R,sd}$  given by

$$p_{R,sd}(x_L, z_L) = \rho_0 c_0 \frac{\gamma^3}{2\pi} \int_{-\infty}^{+\infty} \frac{(k_0 + k_{sd}M)}{2\alpha_{sd}} R(k_{sd}) \frac{dk_{sd}}{dq} e^{iQ(k_s)} e^{-q^2 k_0 r_L} dq e^{-i\omega_0 t_L}, \tag{51}$$

is the contribution of the steepest-descent path to the reflected wave and where  $p_S^\pm$  given by

$$p_S^\pm(x_L, z_L) = \pm 2\pi i a^\pm e^{i\alpha_p^\pm h_L + ik_p^\pm x_L} e^{-i\omega_0 t_L}, \tag{52}$$

are surface waves due to the poles of the reflection coefficient. The parameters  $a^\pm$  are determined from the residues of the poles leading to

$$a^\pm = \rho_0 c_0 \frac{\gamma^3}{2\pi} \frac{\alpha_p^\pm (k_0 + Mk_p^\pm)^2}{k_0 k_p^\pm + Mk_0^2 - \alpha_p^\pm (k_0 + Mk_p^\pm)^2 M \gamma^3 c_0 \beta' [\gamma^2 (\omega_0 + Mc_0 k_p^\pm)]}. \tag{53}$$

where  $\beta'$  is the derivative of the surface admittance with respect to  $\omega$ . Using the relation:

$$\frac{dk_{sd}(q)}{dq} = \frac{2\alpha_{sd}(q)}{\sqrt{2i - q^2}}, \tag{54}$$

the steepest-descent path contribution to the reflected wave is given by

$$p_{R,sd}(x_L, z_L) = \int_{-\infty}^{+\infty} F(q) e^{-q^2 k_0 r_L} dq e^{-i\omega_0 t_L + ik_0 x_L}, \tag{55}$$

with

$$F(q) = \rho_0 c_0 \frac{\gamma^3}{2\pi} \frac{(k_0 + k_{sd}M)}{\sqrt{2i - q^2}} R(k_{sd}). \tag{56}$$

Thus, the integrand does not have anymore the oscillatory behavior of the initial integrand and the evaluation of Eq. (55) can be performed using simple numerical methods such as the trapezoidal rule. However, the contribution from the steepest descent path becomes discontinuous when the poles are crossed. A special attention is then required in that case.

An example of such a case is depicted in Fig. 5, for a line source moving at a Mach number  $M=0.3$  and at a height  $z_s=0.5$  m and emitting at a frequency of  $f_0 = 500$  Hz and for a receiver at a height of  $z=1$  m. The surface admittance is

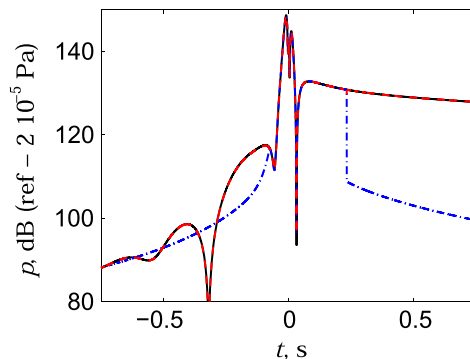


**Fig. 5.** Comparison of the sound pressure level as a function of the time obtained by computing the reflected wave from (black solid) Eq. (33) and from Eq. (50) (blue dash-dotted) neglecting or (red dashed) accounting for the contribution of the surface waves. The source emits at a frequency of 500 Hz and is moving at a Mach number  $M=0.3$  and at a height  $z_s=0.5$  m. The receiver is located at a height  $z=1$  m. The Miki model of a rigidly backed layer of air flow resistivity  $\sigma_0 = 100$  kPa s m<sup>-2</sup> and of thickness  $l=0.01$  m is chosen. (For interpretation of the references to color in this figure caption, the reader is referred to the web version of this paper.)

determined with the Miki model of a rigidly backed layer of air flow resistivity  $\sigma_0 = 100 \text{ kPa s m}^{-2}$  and of thickness  $l = 0.01 \text{ m}$ . Discontinuities of  $p_{R,\text{sd}}$  are clearly observed for  $t = -0.1 \text{ s}$  and  $t = 0.2 \text{ s}$ . As the contributions of the surface waves are added, the solution is in perfect agreement with the analytic solution in Eq. (33). It is also remarked that the contributions of the surface waves are important in this example, as an error of more than 20 dB when neglecting the surface waves is obtained for  $t > 0.2 \text{ s}$ . Indeed, surface waves are likely to be an important contribution to the acoustic pressure for admittance models of a thin, rigidly backed layer [6], such as the one used here.

To derive an asymptotic solution valid in the acoustic far field  $k_0 r_L \gg 1$ , the next step is to apply a Taylor expansion of  $F(q)$  and to carry out the integration in Eq. (55) term by term. The validity of the expansion is however in question, if the poles of the reflection coefficient are located close to the saddle point [20,21]. To remove this restriction, the pole subtraction method is used in the next section.

### 3.4. The method of pole subtraction

The principle of the method is to explicitly remove the poles of the function  $F$ . A Taylor expansion of the remaining term, whose validity is no more restricted by the presence of the poles near the saddle point, can then be performed. Thus, the reflected wave is split into

$$p_R = p_{R,\text{sub}} + p_{R,\text{sd-sub}} + H[\text{Im}(q_p^-)]p_S^- + H[-\text{Im}(q_p^+)]p_S^+ \quad (57)$$

with the new term

$$p_{R,\text{sub}} = \int_{-\infty}^{+\infty} \left[ \frac{a^-}{q - q_p^-} + \frac{a^+}{q - q_p^+} \right] e^{-q^2 k_0 r_L} dq e^{-i\omega_0 t_L + ik_0 r_L}. \quad (58)$$

The integral in the preceding equation can be expressed in terms of elementary functions using the relations [21]

$$\int_{-\infty}^{+\infty} \frac{a^-}{q - q_p^-} e^{-q^2 k_0 r_L} dq = -a^- i\pi e^{-n^-} \left[ \text{erfc}(in^-) - 2H[\text{Im}(q_p^-)] \right], \quad (59)$$

$$\int_{-\infty}^{+\infty} \frac{a^+}{q - q_p^+} e^{-q^2 k_0 r_L} dq = a^+ i\pi e^{-n^+} \left[ \text{erfc}(-in^+) - 2H[-\text{Im}(q_p^+)] \right], \quad (60)$$

where the term  $n^\pm = \sqrt{k_0 r_L} q_p^\pm$  is called the numerical distance and where  $\text{erfc}$  is the complementary error function. The analytic expression of  $p_{R,\text{sub}}$  is then given by

$$p_{R,\text{sub}} = -a^- i\pi e^{-n^-} \text{erfc}(in^-) e^{-i\omega_0 t_L + ik_0 r_L} - H[\text{Im}(q_p^-)]p_S^- + a^+ i\pi e^{-n^+} \text{erfc}(-in^+) e^{-i\omega_0 t_L + ik_0 r_L} - H[-\text{Im}(q_p^+)]p_S^+. \quad (61)$$

It remains to evaluate the integral

$$p_{R,\text{sd-sub}}(x_L, z_L) = \int_{-\infty}^{+\infty} G(q) e^{-q^2 k_0 r_L} dq e^{-i\omega_0 t_L + ik_0 r_L}, \quad (62)$$

with

$$G(q) = F(q) - \frac{a^-}{q - q_p^-} - \frac{a^+}{q - q_p^+}. \quad (63)$$

Unlike  $F$ , the function  $G$  is regular at  $q = q_p^-$  and  $q = q_p^+$ . A Taylor expansion of  $G$  is now applied to get the asymptotic expression. The first term of the expansion is  $G(q=0) = F(q=0) + a^-/q_p^- + a^+/q_p^+$ , which gives after integration:

$$p_{R,\text{sd-sub}}(x_L, z_L) = \rho_0 c_0 \frac{k_0 \gamma^3}{4} \frac{e^{-i\omega_0 t_L + ik_0 r_L}}{\sqrt{ik_0 r_L}} \sqrt{\frac{2}{\pi}} (1 + M \cos \theta_L) R_s + \frac{a^- \sqrt{\pi}}{n^-} e^{-i\omega_0 t_L + ik_0 r_L} + \frac{a^+ \sqrt{\pi}}{n^+} e^{-i\omega_0 t_L + ik_0 r_L}, \quad (64)$$

with the following expression for the reflection coefficient:

$$R_s = R[k_0 \cos \theta_L] = \frac{\sin \theta_L - (1 + M \cos \theta_L) \gamma \beta [\omega_0 \gamma^2 (1 + M \cos \theta_L)]}{\sin \theta_L + (1 + M \cos \theta_L) \gamma \beta [\omega_0 \gamma^2 (1 + M \cos \theta_L)]}. \quad (65)$$

The asymptotic solution for the reflected wave is then

$$p_R(x_L, z_L) = \rho_0 c_0 \frac{k_0 \gamma^3}{4} \frac{e^{-i\omega_0 t_L + ik_0 r_L}}{\sqrt{ik_0 r_L}} \sqrt{\frac{2}{\pi}} (1 + M \cos \theta_L) R_s + \frac{a^- \sqrt{\pi}}{n^-} B(-n^-) e^{-i\omega_0 t_L + ik_0 r_L} + \frac{a^+ \sqrt{\pi}}{n^+} B(n^+) e^{-i\omega_0 t_L + ik_0 r_L}, \quad (66)$$

with the function  $B(n) = 1 + in\sqrt{\pi} \exp(-n^2) \text{erfc}(-in)$ , called the boundary loss factor. The first term in Eq. (66) is the only term which is obtained by the application of the steepest descent method. It represents a ray contribution whose amplitude is modulated by the reflection coefficient evaluated at the saddle point. The two other terms are corrections due to the method of pole subtraction. Compared to the case  $\beta$  constant, there are two modifications: the first one is that the admittance in the reflection coefficient depends on the position of the receiver relative to the source and the second one is that the location of the poles of the reflection coefficient in the  $k$ -plane is not the same.

### 3.5. Approximate formula for a grazing incidence

Approximate formula for a grazing incidence are given in this section first for a constant admittance and second for a frequency-dependent admittance.

#### 3.5.1. Admittance $\beta$ constant with frequency

First, a constant admittance  $\beta(\omega) = \beta(\omega_0)$  is considered. The poles have been already given in Eq. (41). From Eq. (53), the parameters  $a^\pm$  and the numerical distances are obtained by the relation:

$$a^\pm = \pm \rho_0 c_0 \frac{1}{2\pi} \frac{\beta k_0}{\sqrt{1-\beta^2}} \frac{1}{(1 \mp M \sqrt{1-\beta^2})^2}, \tag{67}$$

$$n^\pm = \pm \left[ \frac{ik_0 r_L}{1 \mp M \sqrt{1-\beta^2}} \left( 1 + \mp \left( \sqrt{1-\beta^2} \mp M \right) \cos \theta_L + \frac{\beta}{\gamma} \sin \theta_L \right) \right]^{1/2}. \tag{68}$$

In grazing incidence and for  $|\beta|^2 \ll 1$ , approximate solutions can be given in the form of a classical Weyl–Van der Pol formula, as done for a non-moving source or for a point-source moving at a constant speed parallel to the ground [6]. Thus, the numerical distance  $n^+$  can be expressed for  $\theta_L \approx 0$  and for  $|\beta|^2 \ll 1$  as

$$n^+ = \left[ \frac{ik_0 r_L}{1-M} \left( 1 - \left( 1 - \frac{\beta^2}{2} - M \right) \left( 1 - \frac{\theta_L^2}{2} \right) + \frac{\beta}{\gamma} \theta_L \right) \right]^{1/2}, \tag{69}$$

which is written neglecting the cross term between  $\beta^2$  and  $\theta_L^2$  as

$$n^+ = \left[ \frac{ik_0 r_L}{2} \left( \theta_L^2 + 2\theta_L \beta \gamma (1+M) + \beta^2 \gamma^2 (1+M)^2 \right) \right]^{1/2}. \tag{70}$$

Therefore, the numerical distance  $n^+$  becomes

$$n^+ = \sqrt{\frac{ik_0 r_L}{2}} [\theta_L + (1+M)\gamma\beta] \tag{71}$$

which can be written at first order in  $\theta_L$  and  $\beta$  as

$$n^+ = \sqrt{\frac{ik_0 r_L}{2}} [\sin \theta_L + (1+M \cos \theta_L)\gamma\beta]. \tag{72}$$

For the numerical distance  $n^-$ , one obtains immediately  $n^- = -\sqrt{2ik_0 r_L}$ . Similarly, for  $\theta_L \approx \pi$ , the numerical distance  $n^-$  is given by

$$n^- = -\sqrt{\frac{ik_0 r_L}{2}} [(\pi - \theta_L) + (1-M)\gamma\beta] = -\sqrt{\frac{ik_0 r_L}{2}} [\sin \theta_L + (1+M \cos \theta_L)\gamma\beta], \tag{73}$$

and  $n^+$  is approximated by  $n^+ = \sqrt{2ik_0 r_L}$ .

Concerning the parameters  $a^\pm$ , one can write under the assumption that  $|\beta|^2 \ll 1$ :

$$a^\pm = \pm \rho_0 c_0 \frac{k_0 \beta}{2\pi(1 \mp M)^2} = \pm \frac{\rho_0 c_0}{2\pi} k_0 \beta \gamma^4 (1 \pm M)^2. \tag{74}$$

Moreover, as the asymptotic solution is valid in the acoustic far field  $k_0 r_L \gg 1$ ,  $|n^-|$  and  $|n^+|$  have large values for  $\theta_L \approx 0$  and  $\theta_L \approx \pi$ , respectively. As a consequence, the terms  $B(-n^-)$  are  $B(n^+)$  are very small for  $\theta_L \approx 0$  and  $\theta_L \approx \pi$ , respectively, and can then be neglected. The two last terms in Eq. (66) can be gathered, by writing

$$\frac{a^- \sqrt{\pi}}{n^-} B(-n^-) + \frac{a^+ \sqrt{\pi}}{n^+} B(n^+) = \frac{a \sqrt{\pi}}{n} B(n), \tag{75}$$

with

$$n = \sqrt{\frac{ik_0 r_L}{2}} [\sin \theta_L + (1+M \cos \theta_L)\gamma\beta], \tag{76}$$

$$\frac{a \sqrt{\pi}}{n} B(n) = \rho_0 c_0 \frac{k_0 \gamma^4}{4} \frac{1}{\sqrt{ik_0 r_L}} \sqrt{\frac{2}{\pi}} \frac{2\beta(1+M \cos \theta_L)^2}{\sin \theta_L + (1+M \cos \theta_L)\gamma\beta} B(n). \tag{77}$$

Assuming that  $k_0 r_L \gg 1$  and  $|\beta^2| \ll 1$ , the reflected wave for an admittance which does not depend on the frequency can be written for a grazing incidence in the form

$$p_R(x_L, z_L) = \rho_0 c_0 \frac{k_0 \gamma^3}{4} \frac{e^{-i\omega_0 t_L + ik_0 r_L}}{\sqrt{ik_0 r_L}} \sqrt{\frac{2}{\pi}} (1 + M \cos \theta_L) [R_s + (1 - R_s)B(n)]. \quad (78)$$

Note that no restriction on the Mach number of the source is made to derive this formula.

### 3.5.2. Admittance $\beta$ varying with frequency

As discussed in Section 3.2, it is not possible to give an explicit formula for  $k_p$  and  $\alpha_p$  if the admittance depends on the frequency, as the admittance is a function of  $k$  in the relation  $D(\omega_0, k, M)$ . However, an approximate formula can be given for small Mach numbers. Indeed, the relation  $D(\omega_0, k, M) = 0$  implies the equation

$$(k_0^2 - k^2) - (k_0 + kM)^2 \gamma^2 \beta [(\omega_0 + kc_0 M) \gamma^2]^2 = 0. \quad (79)$$

By linearizing  $\beta[(\omega_0 + kc_0 M) \gamma^2]$  and by keeping only terms in first order in  $M$ , a quadratic equation, whose solutions are

$$k_p^\pm = \pm k_0 \sqrt{1 - \beta^2} - k_0 M (\beta^2 + \omega_0 \beta' \beta), \quad (80)$$

$$\alpha_p^\pm = -k_0 \beta \mp k_0 M (\beta + \omega_0 \beta') \sqrt{1 - \beta^2}, \quad (81)$$

is obtained. The parameters  $k_p^\pm$  and  $\alpha_p^\pm$  now depend on the derivative of the admittance, which modify the location of the poles of the reflection coefficient in the  $k$ -plane. As the expansion order of  $\beta[(\omega_0 + kc_0 M) \gamma^2]$  is increased, higher order derivatives of the admittance would appear. Note also that up to the second order in  $M$ , the linearization of the relation  $D(\omega_0, k, M) = 0$  gives a quadratic equation. This justifies the assumption that for moderate Mach numbers, only two poles of the reflection coefficient are important. At last, it can be remarked that for  $\beta' = 0$ , the solutions given in Eqs. (41) and (42) at the first order are retrieved.

Using the same approach as described in the previous paragraph, an approximate expression of the numerical distances is proposed for a grazing incidence and for  $|\beta|^2 \ll 1$ . For  $\theta_L \approx \pi$ , the numerical distances are approximated by

$$n^- = -\sqrt{\frac{ik_0 r_L}{2}} [(\pi - \theta_L) + \beta - M(\beta + \omega_0 \beta')], \quad (82)$$

$$n^+ = \sqrt{2ik_0 r_L}. \quad (83)$$

The first equation can be rewritten at the first order in  $M$ ,  $\beta$  and  $\theta_L$  as

$$n^- = -\sqrt{\frac{ik_0 r_L}{2}} (\sin \theta_L + \gamma(1 + M \cos \theta_L) \beta [\gamma^2 \omega_0 (1 + M \cos \theta_L)]). \quad (84)$$

For  $\theta_L \approx 0$ , one obtains

$$n^- = -\sqrt{2ik_0 r_L}, \quad (85)$$

$$n^+ = \sqrt{\frac{ik_0 r_L}{2}} [\theta_L + \beta + M(\beta + \omega_0 \beta')]. \quad (86)$$

The numerical distance  $n^+$  can then be written at the first order in  $M$ ,  $\beta$  and  $\theta_L$ , as

$$n^+ = \sqrt{\frac{ik_0 r_L}{2}} (\sin \theta_L + \gamma(1 + M \cos \theta_L) \beta [\gamma^2 \omega_0 (1 + M \cos \theta_L)]). \quad (87)$$

Moreover, the approximate expression of  $a^\pm$  for  $|\beta|^2 \ll 1$  and for low Mach numbers gives

$$a^\pm = \pm \frac{\rho_0 c_0}{2\pi} k_0 (\beta \pm M(2\beta + \omega_0 \beta')). \quad (88)$$

As discussed in the previous paragraph, the contributions due to  $B(-n^-)$  and  $B(n^+)$  can be neglected for  $\theta_L \approx \pi$  and  $\theta_L \approx 0$ , respectively. By introducing

$$\frac{a\sqrt{\pi}}{n} B(n) = \frac{a^+ \sqrt{\pi}}{n^+} B(n^+) + \frac{a^- \sqrt{\pi}}{n^-} B(-n^-), \quad (89)$$

with

$$n = \sqrt{\frac{ik_0 r_L}{2}} (\sin \theta_L + \gamma(1 + M \cos \theta_L) \beta [\gamma^2 \omega_0 (1 + M \cos \theta_L)]), \quad (90)$$

$$\frac{a\sqrt{\pi}}{n} B(n) = \rho_0 c_0 \frac{k_0 \gamma^4}{4} \frac{1}{\sqrt{ik_0 r_L}} \sqrt{\frac{2}{\pi}} \frac{2\beta [\gamma^2 \omega_0 (1 + M \cos \theta_L)] (1 + M \cos \theta_L)^2}{\sin \theta_L + (1 + M \cos \theta_L) \gamma \beta} B(n), \quad (91)$$

the reflected wave can be written for a grazing incidence in the first order in  $\beta$  and in  $M$  as

$$p_R(x_L, z_L) = \rho_0 c_0 \frac{k_0 \gamma^3}{4} \frac{e^{-i\omega_0 t_L + ik_0 r_L}}{\sqrt{ik_0 r_L}} \sqrt{\frac{2}{\pi}} (1 + M \cos \theta_L) [R_s + (1 - R_s)B(n)]. \tag{92}$$

The main interest of this formulation compared to Eq. (66) is that it is not necessary to determine the location of the poles of the reflection coefficient in the complex plane. The solution is similar to Eq. (78) and is obtained by changing  $\beta$  by  $\beta[\gamma^2 \omega_0 (1 + M \cos \theta_L)]$ .

It is also remarked that the asymptotic solutions are in agreement with the comments of Li and Tao [32]. Indeed, the analytical expression obtained for the reflected wave from the pole subtraction method in Eq. (66) depends on numerical distances, based on the location of the poles, which are referred to as apparent numerical distances in [32]. When asymptotic solutions are sought for near-grazing propagation in the form of Weyl–Van der Pol formula, there is a need to introduce an approximate numerical distance, which is given in this study in Eqs. (76) and (90) for an admittance constant with the frequency and for an admittance varying with the frequency, respectively.

### 3.5.3. Expression in the physical coordinates system

The asymptotic solution obtained in the preceding paragraph in the Lorentz space is now written in the physical space. For that, the formulas [8,6]

$$t_L - \frac{d_L}{c_0} = t - \frac{d_e}{c_0}, \tag{93}$$

$$1 + M \cos \psi_L = \frac{1}{\gamma^2 (1 - M \cos \psi_e)}, \tag{94}$$

$$\sin \psi_L = \frac{\sin \psi_e}{\gamma (1 - M \cos \psi_e)}, \tag{95}$$

$$d_L = \gamma^2 d_e (1 - M \cos \psi_e), \tag{96}$$

which relate the variables in the Lorentz space and those in the physical space in retarded time coordinates are used. The retarded time coordinates are determined from the following equations:

$$d_e = \gamma d (\gamma M \cos \psi + \sqrt{1 + \gamma^2 M^2 \cos^2 \psi}), \tag{97}$$

$$\cos \psi_e = M + d/d_e \cos \psi, \tag{98}$$

$$\sin \psi_e = d/d_e \sin \psi, \tag{99}$$

with  $d = \sqrt{(x - V_s t)^2 + (z - z_s)^2}$ ,  $\cos \psi = x/d$  and  $\sin \psi = (z - z_s)/d$ . Relations have been given only for the physical coordinates centered at the source. Those centered at the image source are obtained by changing  $-z_s$  by  $z_s$  in the preceding formula. From Eqs. (35) and (92), the solution is then written as

$$p(x, z, t) = \rho_0 c_0 \frac{k_0}{4} \frac{e^{-i\omega_0 t + ik_0 d_e}}{\sqrt{ik_0 d_e} (1 - M \cos \psi_e)^{3/2}} \sqrt{\frac{2}{\pi}} + \rho_0 c_0 \frac{k_0}{4} \frac{e^{-i\omega_0 t + ik_0 r_e}}{\sqrt{ik_0 r_e} (1 - M \cos \theta_e)^{3/2}} \sqrt{\frac{2}{\pi}} [R_s + (1 - R_s)B(n)], \tag{100}$$

where the reflection coefficient and the numerical distance are expressed in the form

$$R_s = \frac{\sin \theta_e - \beta[\omega_0 / (1 - M \cos \theta_e)]}{\sin \theta_e + \beta[\omega_0 / (1 - M \cos \theta_e)]}, \tag{101}$$

$$n = \sqrt{\frac{ik_0 r_e}{2(1 - M \cos \theta_e)}} (\sin \theta_e + \beta[\omega_0 / (1 - M \cos \theta_e)]). \tag{102}$$

Eq. (100) can be called the Doppler Weyl–Van der Pol formula for the 2D-case, with reference to the solution proposed for a point-source moving above a plane with a constant impedance by Attenborough et al. [6]. The direct wave corresponds to the solution obtained for a line source in uniform motion in free field and in acoustic far field [33]. In particular, the exponent of the Doppler factor in the convective amplification term is 3/2, instead of 2 for a point-source. This is also the case for the reflected wave. The reflection coefficient in Eq. (101) has a simpler form than in the Lorentz space. It is the same expression than that for a non-moving source except that the admittance is not evaluated at the emitting frequency but at the Doppler frequency  $f_0 / (1 - M \cos \theta_e)$ .

## 4. Comparison with a numerical solution

In order to validate the asymptotic solutions derived in the previous section, a comparison with a numerical solution obtained from a solver of the linearized Euler equations is now performed. The solver is presented in [34]. High-order numerical schemes [35] are employed. A time-domain impedance boundary condition [31] based on a recursive convolution

method is used to account for reflexion of acoustic waves on the ground. The solver has been validated against several test-cases and experimental data obtained from outdoor measurements performed on a complex site [36].

The source is implemented through the mass source term. The spatial distribution of the source is a Gaussian:

$$Q(\mathbf{x}) = \frac{1}{\pi B^2} \exp\left(-\frac{|\mathbf{x}|^2}{B^2}\right), \quad (103)$$

which tends to the Dirac delta function  $\delta(\mathbf{x})$  as the radius  $B$  tends to 0. Two examples are considered. In the first case, the emitting frequency is  $f_0 = 200$  Hz and the surface admittance model is the Miki model for a semi-infinite ground of air flow resistivity  $\sigma_0 = 500$  kPa s m<sup>-2</sup>. In the second case, the source frequency is  $f_0 = 500$  Hz and the Miki model of a rigidly backed layer of thickness  $l = 0.01$  m and of air flow resistivity  $\sigma_0 = 100$  kPa s m<sup>-2</sup> is chosen. In both cases, the source is moving at a speed  $V_s = 100$  m s<sup>-1</sup> and at a height  $z_s = 0.5$  m. The receiver is located at  $x = 0$  m and  $z = 2$  m. The grid is uniform with a spatial step equal to  $\Delta x = \Delta z = 0.01$  m. The Courant–Friedrichs–Lewy number, defined by  $CFL = c_0 \Delta t / \Delta x$  is set to 0.8, and more than 40 000 time iterations are performed. The domain size is  $[-60 \text{ m}, 50 \text{ m}] \times [0 \text{ m}, 6 \text{ m}]$ . The source is located at the initial simulation time at  $x_s = -50$  m. In addition, the radius of the Gaussian is  $B = 0.024$  m. For the largest frequency of interest, the parameter  $k_0 B = 0.2$  is small compared to one. Thus, the source can be considered as compact and is expected to behave as a line source.

The sound pressure levels obtained from the numerical solution and from the analytical solution given in Eqs. (32) and (33) are displayed in Fig. 6 as a function of the time. For both cases, a very good agreement is found. The analytical solution obtained for a constant surface admittance is represented with a blue dash-dotted line. A deviation of about 0.5 dB is obtained from the reference solution for the first admittance model in Fig. 6(a) as the source approaches the receiver. As the source recedes from the receiver, the analytical solutions for a constant surface admittance and for a surface admittance varying with the frequency are almost superimposed. For the second model in Fig. 6(b), the deviation is larger, of about 4 dB. Moreover, a destructive interference pattern is observed around  $t = -0.1$  s if the surface admittance does not depend on the frequency and is not predicted if the variation of the admittance with the frequency is accounted for.

The asymptotic solutions obtained by computing the reflected wave with Eqs. (66) and (100) have been represented in Fig. 7 as a function of the time along with the analytical solution in the integral form given in Eqs. (32) and (33). For both cases, the curves are almost superimposed, which shows the accuracy of the asymptotic solutions.

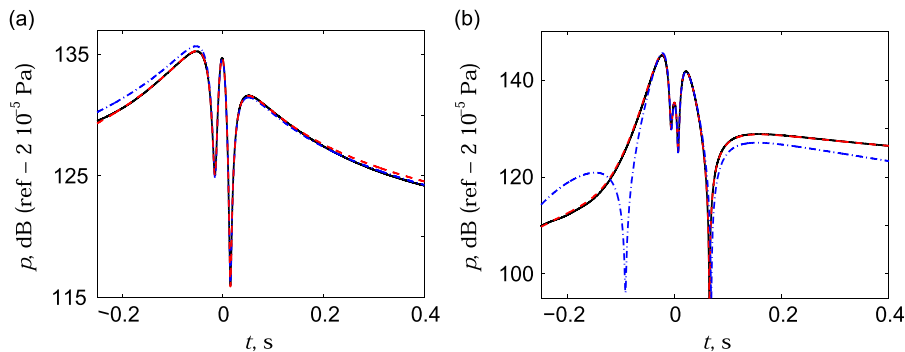


**Fig. 6.** Comparison of the sound pressure level as a function of the time obtained from (black solid) the numerical solution and (red dashed) the analytical solution computed from Eqs. (32) and (33) for the set of parameters (a)  $\sigma_0 = 500$  kPa s m<sup>-2</sup>,  $l = \infty$  and  $f_0 = 200$  Hz and (b)  $\sigma_0 = 100$  kPa s m<sup>-2</sup>,  $l = 0.01$  m and  $f_0 = 500$  Hz. The dash-dotted blue line represents the analytical solution obtained for a constant surface admittance. The source is moving at a speed  $V_s = 100$  m s<sup>-1</sup> and at a height  $z_s = 0.5$  m. The receiver is located at a height  $z = 2$  m. (For interpretation of the references to color in this figure caption, the reader is referred to the web version of this paper.)

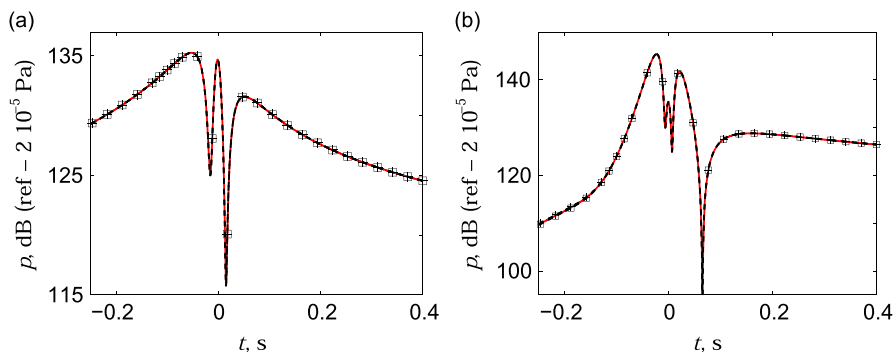


**Fig. 7.** Comparison of the sound pressure level as a function of the time obtained by computing the reflected wave from (red solid) the analytical solution in Eq. (33) and (black dashed) the asymptotic solutions ( $\square$ ) in Eq. (66) and ( $+$ ) Eq. (100) for the set of parameters (a)  $\sigma_0 = 500$  kPa s m<sup>-2</sup>,  $l = \infty$  and  $f_0 = 200$  Hz and (b)  $\sigma_0 = 100$  kPa s m<sup>-2</sup>,  $l = 0.01$  m and  $f_0 = 500$  Hz. The source is moving at a speed  $V_s = 100$  m s<sup>-1</sup> and at a height  $z_s = 0.5$  m. The receiver is located at a height  $z = 2$  m. (For interpretation of the references to color in this figure caption, the reader is referred to the web version of this paper.)

### 5. Importance of accounting for the frequency variation of $\beta$

The importance of accounting for the frequency variation of admittance models is now studied for various configurations. The parameter of interest is the difference  $\Delta L$  between the sound pressure obtained from the analytical solutions for a frequency-dependent admittance  $\beta = \beta(\omega)$ , denoted by  $p_\omega$ , and for a constant admittance  $\beta = \beta(\omega_0)$ , denoted by  $p_{\omega_0}$ . To avoid any interference effect,  $\Delta L$  is computed on 1/3 octave bands from

$$\Delta L(f_c) = 20 \log_{10} \left( \frac{\langle p_\omega \rangle_{f_c}}{\langle p_{\omega_0} \rangle_{f_c}} \right), \tag{104}$$

where  $\langle \rangle_{f_c}$  means the integrated value over the 1/3 octave band centered at  $f_c$ . The reference configuration corresponds to a source moving at a Mach number  $M=0.3$  and at a height  $z_s=0.5$  m above an admittance plane whose admittance is given by the modified Miki model (see. Eq. (45)) for  $\sigma_0 = 100 \text{ kPa s m}^{-2}$  and  $l=0.01$  m, which are typical values for a grassy ground [24]. First, the influence of the source speed is investigated by comparing  $\Delta L$  for three Mach numbers  $M=0.1, 0.2$  and  $0.3$ . Second, the role of the ground properties is examined and three sets of coefficients of the Miki model are considered ( $\sigma_0 = 100 \text{ kPa s m}^{-2}, l=0.01$  m), ( $\sigma_0 = 200 \text{ kPa s m}^{-2}, l=0.01$  m) and ( $\sigma_0 = 100 \text{ kPa s m}^{-2}, l = \infty$ ). Third, the influence of the source height is investigated. For that, the source is positioned at three heights:  $z_s=0.5$  m, 1 m and 4 m. In all configurations, the receiver is located at  $x=0$  m and  $z=2$  m. At the time origin  $t=0$  s, the source is located at ( $x_s=0$  m,  $z_s$ ).

#### 5.1. Influence of the source speed

It is expected that the differences between the analytical solutions for  $\beta$  constant and for  $\beta = \beta(\omega)$  increase as the source speed increases, because the Doppler shift becomes more and more pronounced, as the Mach number increases. To confirm this point,  $\Delta L$  is represented as a function of the time for three 1/3 octave bands and for the three Mach numbers in Fig. 8.

For the 1/3 octave band centered at 400 Hz,  $\Delta L$  is larger for  $M=0.3$  and for  $t < 0$ , during the approach phase. The maximal difference is 20 dB and is obtained for  $t = -0.9$  s. This difference decreases as  $M$  decreases. Thus, for  $M=0.2$  and  $M=0.1$ , it is reduced to 10 dB and 2 dB, respectively. The same conclusions apply for the 1/3 octave band centered at 630 Hz. At higher frequencies, for the 1/3 octave band centered at 1600 Hz,  $\Delta L$  has smaller values, around 2 dB at maximum. This behavior can be explained as the variations of the admittance model are small at high frequencies, which therefore imply that the approximation  $\beta(\omega) = \beta(\omega_0)$  is correct in that case.

#### 5.2. Influence of the ground parameters

The influence of the ground parameters on  $\Delta L$  is now investigated. For that,  $\Delta L$  is represented as a function of the time for the three sets of ground parameters and for three 1/3 octave bands in Fig. 9. For the first one centered at 160 Hz,  $\Delta L$  is small when considering a ground layer of finite thickness  $l$ , while it has a large value, around 5 dB, for  $l$  infinite. At higher frequencies, the opposite behavior is observed. Indeed, for the 1/3 octave band centered at 400 Hz,  $\Delta L$  is small for the semi-infinite ground and is large for  $l$  finite. Finally, for the 1/3 octave band centered at 1600 Hz, the values of  $\Delta L$  are almost the same for the three sets of ground parameters. This shows that differences from the approximation  $\beta(\omega) = \beta(\omega_0)$  depend strongly on the ground parameters.

#### 5.3. Influence of the geometry

The role of the source height on  $\Delta L$  is now studied. In Fig. 10,  $\Delta L$  is plotted as a function of the time for the three source heights and for three 1/3 octave bands. For the one centered at 400 Hz, the maximal value of  $\Delta L$  decreases as the source

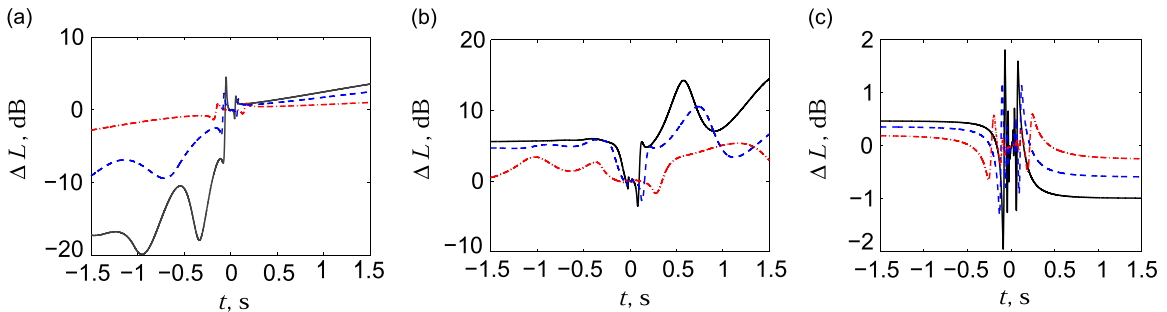


**Fig. 8.**  $\Delta L$  in dB as a function of the time for a source moving at a height  $z_s=0.5$  m and at a Mach number  $M=0.1$  (red dash-dotted),  $M=0.2$  (blue dashed) and  $M=0.3$  (black solid) and for the 1/3 octave bands centered at (a) 400 Hz, (b) 630 Hz and (c) 1600 Hz. The receiver is located at  $x=0$  m and  $z=2$  m and the surface admittance model is the Miki model of a rigidly backed layer with  $\sigma_0 = 100 \text{ kPa s m}^{-2}$  and  $l=0.01$  m. (For interpretation of the references to color in this figure caption, the reader is referred to the web version of this paper.)

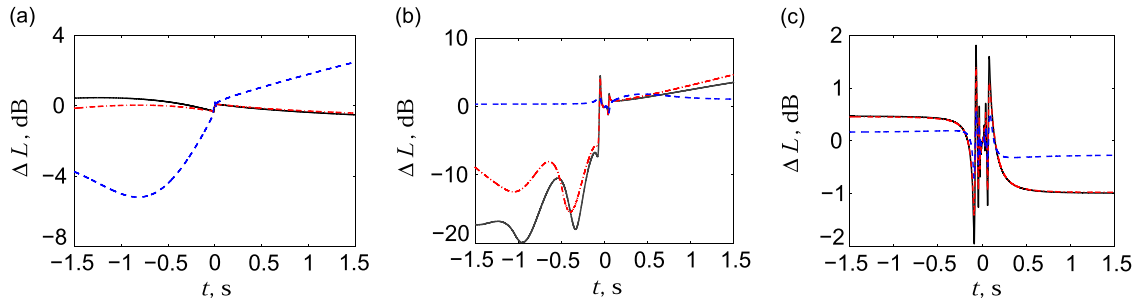


**Fig. 9.**  $\Delta L$  in dB as a function of the time for three sets of ground parameters of the Miki admittance model, ( $\sigma_0 = 100 \text{ kPa m s}^{-2}$ ,  $l = 0.01 \text{ m}$ ) (black solid), ( $\sigma_0 = 200 \text{ kPa m s}^{-2}$ ,  $l = 0.01 \text{ m}$ ) (red dash-dotted) and ( $\sigma_0 = 100 \text{ kPa m s}^{-2}$ ,  $l = \infty$ ) (blue dashed) and for the 1/3 octave bands centered at (a) 160 Hz, (b) 400 Hz and (c) 1600 Hz. The source is moving at a height  $z_S = 0.5 \text{ m}$  and at a Mach number  $M = 0.3$  and the receiver is located at  $x = 0 \text{ m}$  and  $z = 2 \text{ m}$ . (For interpretation of the references to color in this figure caption, the reader is referred to the web version of this paper.)

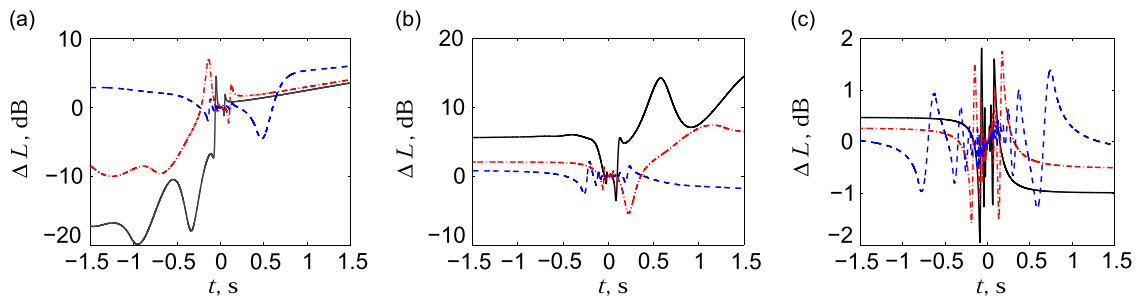


**Fig. 10.**  $\Delta L$  in dB as a function of the time for a source moving at a Mach number  $M = 0.3$  and at a height  $z_S = 0.5 \text{ m}$  (black solid),  $z_S = 1 \text{ m}$  (red dash-dotted) and  $z_S = 4 \text{ m}$  (blue dashed) and for the 1/3 octave bands centered at (a) 400 Hz, (b) 630 Hz and (c) 1600 Hz. The receiver is located at  $x = 0 \text{ m}$  and  $z = 2 \text{ m}$  and the Miki admittance model with  $\sigma_0 = 100 \text{ kPa m s}^{-2}$  and  $l = 0.01 \text{ m}$  is used. (For interpretation of the references to color in this figure caption, the reader is referred to the web version of this paper.)

height increases. It is thus 20 dB for  $z_S = 0.5 \text{ m}$ , but reduces to 10 dB and 6 dB for  $z_S = 1 \text{ m}$  and  $z_S = 4 \text{ m}$ , respectively. The same behavior is retrieved for the 1/3 octave band centered at 630 Hz. However, this is not the case for the 1/3 octave band centered at 1600 Hz as the maximal difference is almost the same for the three source heights. In addition, oscillations with amplitudes of about 1 dB are observed in Fig. 10(c) for a source height of  $z_S = 4 \text{ m}$ . They are due to the modification of the interference locations, as from Eq. (101) the reflection coefficient is changed by the source motion. As the source height increases, more and more interferences are present, which produces the oscillations observed on  $\Delta L$ . To summarize, accounting for the frequency variation of the admittance is required if the source is close to the ground. If the source height is large enough, ground effects are less pronounced and the assumption  $\beta$  constant gives accurate results.

## 6. Conclusion

An analytic solution for the problem of sound radiation by a harmonic line source moving at a uniform subsonic speed parallel to an impedance plane has been presented. For that, a modified Lorentz transformation has been used and the time-domain impedance boundary condition has been carefully written in the Lorentz space. Unlike previous solutions developed in the literature for a point-source, the frequency variation of the ground properties has been accounted for. This modifies the reflection coefficient and the location of its poles in the complex plane. Moreover, uniform asymptotic expressions have been proposed in the acoustic far field for moderate Mach numbers. In addition, an approximate expression has been deduced for a grazing incidence for hard grounds and for low Mach numbers in the form of a Weyl–Van der Pol formula. It has been shown that the reflected wave is a function of the impedance evaluated at the Doppler frequency instead of the source frequency. To validate the analytical solutions, a comparison has then been performed with a numerical solution obtained from a time-domain solver of the linearized Euler equations. A satisfactory agreement has been found. Finally, various configurations have been investigated to study the influence of approximating the impedance as a constant. It was shown that this approximation gives good estimates if the source height is sufficiently large, typically larger than 2 m, or if the Mach number remains small, typically smaller than 0.2. Therefore, it is appropriate for studies of road traffic noise, as the Mach number of road vehicles is usually smaller than 0.15. However, the frequency variation of the surface impedance must be typically accounted for in railway noise applications, in which Mach numbers usually exceed 0.2 and acoustic sources are close to the ground.

In addition, the analytic solutions can be used as a benchmark for time-domain propagation codes. A direct extension of this work would be to investigate the case a point-source in uniform motion parallel to an impedance plane with a frequency-dependent impedance.

## Acknowledgments

The work was granted access to the HPC resources of IDRIS under the allocation 2014-022203 made by GENCI (Grand Equipement National de Calcul Intensif). It was performed within the framework of the Labex CeLyA of Université de Lyon, operated by the French National Research Agency (ANR-10-LABX-0060/ ANR-11-IDEX-0007).

## References

- [1] D. Dagna, P. Blanc-Benon, F. Poisson, Modeling of broadband moving sources for time-domain simulations of outdoor sound propagation, *AIAA Journal* 52 (9) (2014) 1928–1939.
- [2] D. Dagna, P. Blanc-Benon, Towards realistic simulations of sound radiation by moving sources in outdoor environments, *International Journal of Aeroacoustics* 13 (5–6) (2014) 405–426.
- [3] T.D. Norum, C.H. Liu, Point source moving above a finite impedance reflecting plane—experiment and theory, *Journal of the Acoustical Society of America* 63 (4) (1978) 1069–1073.
- [4] S. Oie, R. Takeuchi, Sound radiation from a point source moving in parallel to a plane surface of porous material, *Acustica* 48 (3) (1981) 123–129.
- [5] T.F.W. Embleton, Tutorial on sound propagation outdoors, *Journal of the Acoustical Society of America* 100 (1) (1996) 31–48.
- [6] K. Attenborough, K.M. Li, K. Horoshenkov, *Predicting Outdoor Sound*, Taylor & Francis, London and New York, 2007, pp. 25–65 and 191–228 (Chapters 2 and 7).
- [7] M. Ochmann, Exact solutions for sound radiation from a moving monopole above an impedance plane, *Journal of the Acoustical Society of America* 133 (4) (2013) 1911–1921.
- [8] P.M. Morse, K.U. Ingard, *Theoretical Acoustics*, McGraw-Hill, New York, 1968, pp. 717–737 (Section 11.2).
- [9] M. Abramowitz, I. Stegun, *Handbook of Mathematical Functions*, Dover, New York, 1965, p. 364 (formula 9.2.3).
- [10] K.U. Ingard, On the reflection of a spherical sound wave from an infinite plate, *Journal of the Acoustical Society of America* 23 (3) (1951) 329–335.
- [11] A.R. Wenzel, Propagation of waves along an impedance boundary, *Journal of the Acoustical Society of America* 55 (5) (1974) 956–963.
- [12] C.F. Chien, W.W. Soroka, Sound propagation along an impedance plane, *Journal of Sound and Vibration* 43 (1) (1975) 9–20.
- [13] R.J. Donato, Propagation of a spherical wave near a plane boundary with a complex impedance, *Journal of the Acoustical Society of America* 60 (1) (1976) 34–39.
- [14] S.-I. Thomasson, Reflection of waves from a point source by an impedance boundary, *Journal of the Acoustical Society of America* 55 (5) (1974) 780–785.
- [15] S.N. Chandler-Wilde, D.C. Hothersall, A uniformly valid far field asymptotic expansion of the Green function for two-dimensional propagation above a homogeneous impedance plane, *Journal of Sound and Vibration* 182 (5) (1995) 665–675.
- [16] K.M. Li, S. Taherzadeh, K. Attenborough, Sound propagation from a dipole source near an impedance plane, *Journal of the Acoustical Society of America* 101 (6) (1997) 3343–3352.
- [17] K.M. Li, S. Taherzadeh, The sound field of an arbitrarily oriented quadrupole near ground surfaces, *Journal of the Acoustical Society of America* 102 (4) (1997) 2050–2057.
- [18] E.J. Brambley, G. Gabard, Reflection of an acoustic line source by an impedance surface with uniform flow, *Journal of Sound and Vibration* 333 (21) (2014) 5548–5565.
- [19] F.G. Leppington, Asymptotic evaluation of integrals, in: D.G. Crighton, A.P. Dowling, J.E. Ffowcs Williams, M. Heckl, F.G. Leppington (Eds.), *Modern Methods in Analytical Acoustics*, Springer-Verlag, London 1992, pp. 124–147.
- [20] L.B. Felsen, N. Marcuvitz, *Radiation and Scattering of Waves*, IEEE Press, 1994, pp. 370–442 (Section 4).
- [21] L.M. Brekhovskikh, O.A. Godin, *Acoustics of Layered Media II*, second edition, Springer-Verlag, Berlin, Heidelberg, New York, 1999 (Appendix A, Formula A.3.4).
- [22] Y. Miki, Acoustical properties of porous materials—modifications of Delany–Bazley models, *Journal of the Acoustical Society of Japan* 11 (1) (1990) 19–24.
- [23] D. Dagna, P. Blanc-Benon, Physically admissible impedance models for time-domain computations of outdoor sound propagation, *Acta Acustica united with Acustica* 100 (3) (2014) 401–410.
- [24] K. Attenborough, I. Bashir, S. Taherzadeh, Outdoor ground impedance models, *Journal of the Acoustical Society of America* 129 (5) (2011) 521–544.
- [25] D.K. Wilson, Simple relaxational models for the acoustical properties of porous media, *Applied Acoustics* 50 (1997) 171–188.
- [26] J. Defrance, E. Salomons, N. Noordhoek, D. Heimann, B. Plovsing, G. Watts, H. Jonasson, H. Zhang, E. Premat, I. Schmich, F. Aballea, M. Baulac, B. de Roo, Outdoor sound propagation reference model developed in the European Harmonoise project, *Acta Acustica united with Acustica* 93 (2) (2007) 213–227.
- [27] S.W. Rienstra, Impedance models in time domain including the Helmholtz resonator model, Twelfth AIAA/CEAS Aeroacoustics Conference, Cambridge, MA, USA, AIAA Paper 2006–2686, 2006.
- [28] R. Raspet, G.E. Baird, W. Wu, The relationship between upward refraction above a complex impedance plane and the spherical wave evaluation for a homogeneous atmosphere, *Journal of the Acoustical Society of America* 89 (1) (1991) 107–114.
- [29] S.N. Chandler-Wilde, K.V. Horoshenkov, Padé approximants for the acoustical characteristics of rigid frame porous media, *Journal of the Acoustical Society of America* 98 (2) (1995) 1119–1129.
- [30] V.E. Ostashev, S.L. Collier, D.K. Wilson, D.F. Aldridge, N.P. Symons, D.H. Marlin, Padé approximation in time-domain boundary conditions of porous surfaces, *Journal of the Acoustical Society of America* 122 (1) (2007) 107–112.
- [31] B. Cotté, P. Blanc-Benon, C. Bogey, F. Poisson, Time-domain impedance boundary conditions for simulations of outdoor sound propagation, *AIAA Journal* 47 (10) (2009) 2391–2403.
- [32] K.M. Li, H. Tao, Heuristic approximations for sound fields produced by spherical waves incident on locally and non-locally reacting planar surfaces, *Journal of the Acoustical Society of America* 135 (1) (2014) 58–66.
- [33] K. Tanaka, S. Ishii, Acoustic radiation from a moving line source, *Journal of Sound and Vibration* 77 (3) (1981) 397–401.
- [34] D. Dagna, P. Blanc-Benon, F. Poisson, Time-domain solver in curvilinear coordinates for outdoor sound propagation over complex terrain, *Journal of the Acoustical Society of America* 133 (6) (2013) 3751–3763.
- [35] C. Bogey, C. Bailly, A family of low dispersive and low dissipative explicit schemes for flow and noise computations, *Journal of Computational Physics* 194 (2004) 194–214.
- [36] D. Dagna, P. Blanc-Benon, F. Poisson, Impulse propagation over a complex site: a comparison of experimental results and numerical predictions, *Journal of the Acoustical Society of America* 135 (3) (2014) 1096–1105.